Self-entrainment of the right and left vocal fold oscillators

Jorge C. Lucero[a)]
Department of Computer Science, University of Brasilia, Brasilia, Federal District, 70910-900, Brazil

Jean Schoentgen
Laboratories of Image, Signal Processing and Acoustics, Université Libre de Bruxelles, Faculty of Applied Sciences 50, Avenue Franklin D. Roosevelt, B-1050, Brussels, Belgium

Jessy Haas, Paul Luizard, and Xavier Pelorson
Grenoble Images Parole Signal Automatique, Unité Mixte de Recherche 5216, Centre National de la Recherche Scientifique, Grenoble Universities, 961 rue de la Houille Blanche, BP 46, 38402 Saint-Martin d'Heres, France

This article presents an analysis of entrained oscillations of the right and left vocal folds in the presence of asymmetries. A simple one-mass model is proposed for each vocal fold. A stiffness asymmetry and open glottis oscillations are considered first, and regions of oscillation are determined by a stability analysis and an averaging technique. The results show that the subglottal threshold pressure for 1:1 entrainment increases with the asymmetry. Within that region, both folds oscillate with the same amplitude and with the lax fold delayed in time with regard to the tense fold. At large asymmetries, a region involving several different phase entrainments or toroidal regimes at constant threshold pressure appears. The effect of vocal fold collisions and asymmetry in the damping coefficients of the oscillators are explored next by means of numerical analyses. It is shown that the damping asymmetry expands the 1:1 entrainment region at low subglottal pressures across the whole asymmetry range. In the expanded region, the oscillator with the lowest natural frequency is dominant and the other oscillator has a large phase advance and small amplitude. The theoretical results are finally compared with data collected from a mechanical replica of the vocal folds. © 2015 Acoustical Society of America.
[http://dx.doi.org/10.1121/1.4916601]

I. INTRODUCTION

The right and left vocal folds constitute a pair of coupled biomechanical oscillators, where the coupling is provided mainly by interaction with the airflow through the glottis and by collision between the folds during the oscillatory cycle. In normal conditions, anatomical differences between the oscillators are small enough so that they are self-entrained in complete in-phase synchrony, i.e., they oscillate with a common frequency and similar phase (Titze, 1994). Tissue lesions, neurological disorders, and other abnormalities introduce right–left asymmetries, which may cause a phase difference between the vocal folds (Schwarz *et al.*, 2006; Zhang *et al.*, 2013), oscillations at various phase entrainment regimes (Eysholdt *et al.*, 2003; Mergell *et al.*, 2000; Zhang, 2010), quasi-periodic oscillations (Tigges *et al.*, 1997; Wilden *et al.*, 1998), and irregular (possible chaotic) oscillations (Berry *et al.*, 1996).

Let us recall here that two oscillators are in an *n:m* phase entrainment regime if their respective phases, denoted as $\varphi_{1,2}(t)$, satisfy $|n\varphi_1 - m\varphi_2| < M$, where M is a constant and *n,m* are integers (Pikovsky *et al.*, 2001). In the past decades, several theoretical models have been proposed to characterize the entrainment dynamics of asymmetric vocal folds (e.g., Erath *et al.*, 2013; Herzel and Knudsen, 1995; Ishizaka and Isshiki, 1976; Mergell and Herzel, 1997; Smith *et al.*, 1992; Steinecke and Herzel, 1995; Zhang and Jiang, 2004; Zhang and Luu, 2012). Among them, a popular and simple model has been the asymmetric two-mass model (Steinecke and Herzel, 1995), in which each vocal fold is represented as a coupled two-mass oscillator and an asymmetry is introduced in the natural frequencies. In general, the models have revealed a rich variety of nonlinear phenomena that match reported experimental observations. However, such a dynamics is still far from being completely understood (Zhang, 2010). In fact, inconsistencies of past results regarding characteristics of amplitude and phase of the asymmetric oscillations have been reported (Zhang and Luu, 2012). Considering a tense fold vs a lax fold (as in a unilateral paralysis), it is not clear whether the lax fold precedes the tense fold in phase during the oscillation, or the tense precedes the lax fold. Also, studies have reported either oscillation with similar amplitudes for both folds or one of the folds with greater amplitude than the other (see Zhang and Luu, 2012, for a detailed discussion of the inconsistencies). It has also been shown that several of the nonlinear phenomena found in the asymmetric two-mass model are actually artifacts owing to modeling limitations of the forcing functions (Erath *et al.*, 2013). When the limitations are removed, several

---

[a)]Author to whom correspondence should be addressed. Electronic mail: lucero@unb.br

regions of $n{:}m$ phase entrainment disappear, and the model oscillates in either 1:1 or 1:2 regimes.

An additional interesting phenomenon has been recently detected in experiments with a physical model of the vocal folds (Zhang and Luu, 2012; Zhang *et al.*, 2013). At feeble asymmetries, both folds oscillate in 1:1 entrainment with similar amplitudes and with the stiffer fold leading in phase. When the asymmetry is increased, the vocal folds turn to a different oscillatory regime, where the lax fold dominates. In this regime, the frequency is lower and determined by the lax fold, and the stiff fold follows the lax one in anti-phase with much smaller amplitude. The phenomenon was reproduced by numerical simulations on a vocal fold model and described in terms of eigenmode synchronization. However, a clearer picture of its dynamics would be desirable.

The purpose of this article is to investigate the dynamics of right–left vocal fold entrainment by using a simple model. The model is related to the classical van der Pol oscillator (Cartwright, 1960) and also to Adler's equation of phase dynamics (Adler, 1946), both ubiquitous in oscillatory systems studied in mathematical physiology (e.g., Glass, 2001; Glass and Mackey, 1988; Edelstein-Keshet, 2005). The model is first developed and analyzed using standard stability analysis and perturbation techniques. Next, its behavior in more complex configurations is explored using numerical solutions. Finally, the theory is compared with data measured on a mechanical replica of the vocal folds.

II. MODEL

A. Basic equations

Following previous work (Laje *et al.*, 2001; Lucero *et al.*, 2011), each vocal fold is represented by a lumped mass-damper-spring oscillator of the form

$$M\ddot{x}_r + B(1 + \eta x_r^2)\dot{x}_r + Kx_r = P_g, \qquad (1)$$

where x_r is the tissue displacement of the right vocal fold, M, B, and K are the mass, damping, and stiffness, respectively, per unit area of the vocal fold medial surface, η is a nonlinear coefficient to account for energy dissipation at large amplitudes, and P_g is the glottal mean air pressure. The left vocal fold is modeled with a similar equation in the variable x_ℓ.

The glottal airflow is assumed frictionless, stationary, and incompressible. Up to the glottal exit, the airflow follows Bernoulli's law, and at the glottal exit all the flow energy is lost due to turbulence. For simplicity, all the loads presented by the sub- and supraglottal systems are neglected. In this way, any effect of the vocal tract-source interaction on the oscillation dynamics is eliminated. Therefore, the subglottal pressure P_s is assumed equal to a constant lung pressure, and the pressure at the glottal exit is atmospheric. Under these conditions, the glottal mean air pressure may be simply expressed by

$$P_g = P_s\left(\frac{a_1 - a_2}{a_1}\right), \quad a_1, a_2 > 0, \qquad (2)$$

where P_s is the subglottal pressure and a_1 and a_2 are the cross-sectional glottal areas at the lower and upper edges of the vocal folds, respectively. Further, the glottal areas are given by

$$a_{1,2}(t) = L[2x_0 + x_r(t \pm \tau) + x_\ell(t \pm \tau)], \qquad (3)$$

where L is the vocal fold length, x_0 is the half glottal width at rest (prephonatory position), and τ is the time delay for the surface wave to travel half the glottal height T.

Assuming τ is small enough, the approximation $x(t \pm \tau) \approx x(t) \pm \tau\dot{x}(t)$ may be used, which produces

$$P_g = 2\tau P_s\left(\frac{\dot{x}_r + \dot{x}_\ell}{2x_0 + x_r + x_\ell}\right), \qquad (4)$$

and reduces the model to an ordinary differential equation.

The symmetric case, with $x_r = x_\ell$, has been thoroughly analyzed in previous works under a variety of configurations (e.g., Lucero *et al.*, 2011), and it has been found to provide a good characterization of experimental data from both human subjects (Lucero *et al.*, 2012a) and mechanical replicas of the vocal folds (Lucero *et al.*, 2012b).

The model may be further simplified by approximating P_g by its linearization around $x_{r,\ell} = 0$, $\dot{x}_{r,\ell} = 0$, which produces

$$M\ddot{x}_r + B(1 + \eta x_r^2)\dot{x}_r + Kx_r = \frac{\tau P_s}{x_0}(\dot{x}_r + \dot{x}_\ell). \qquad (5)$$

Finally, letting $\beta = B/\sqrt{KM}$, $\alpha = \tau P_s/(x_0\sqrt{MK})$, and applying the substitutions $t \to (\sqrt{M/K})t$, $x_{r,\ell} \to \sqrt{\eta}x_{r,\ell}$, yields

$$\ddot{x}_r + \beta(1 + x_r^2)\dot{x}_r + x_r = \alpha(\dot{x}_r + \dot{x}_\ell). \qquad (6)$$

It might seem that the linear approximation of the glottal pressure would introduce an extreme simplification of the oscillatory dynamics. However, we claim that Eq. (6) is an elegant and convenient representation of the vocal oscillator for the present study, and this for a number of reasons. First, it may be put into the form of a van der Pol oscillator

$$\ddot{x}_r - \beta(\lambda - x_r^2)\dot{x}_r + x_r = \alpha(\dot{x}_\ell - \dot{x}_r), \qquad (7)$$

where $\lambda = (2\alpha - \beta)/\beta$. This form allows for the application of the extensive available theory on van der Pol oscillators (e.g., Grimshaw, 1991) to the study of phonation. For instance, in the symmetrical case of $x_r = x_\ell$, the theory tells us that a supercritical Hopf bifurcation occurs at $\lambda = 0$, which implies $\alpha = \beta/2$ and therefore $P_s = x_0 B/(2\tau)$. This critical value of P_s is known as the phonation threshold pressure (Titze, 1992). The van der Pol characterization has also been extensively used in the context of syrinx modeling for birdsong production (Laje *et al.*, 2002; Arneodo and Mindlin, 2009), and it has been found to reproduce the main dynamic features of the oscillation with no significant differences over the original Eq. (2) for P_g.

To have a reference for possible values of parameters α and β, let us consider a normal voice in a male adult configuration, with $M = 0.5 \text{ g/cm}^2$, $B = 100 \text{ dyne s/cm}^3$, $K = 200\,000 \text{ dyne/cm}^3$, $\tau = 1 \text{ ms}$, $x_0 = 0.1 \text{ cm}$, and $P_s = 800 \text{ Pa}$ (Titze, 1988). Those values produce $\beta = 0.32$ and $\alpha = 0.25$. Note that β is small ($\beta < 1$), therefore the oscillator does not behave as a relaxation oscillator. Instead, it is a quasi-linear oscillator with a nearly harmonic solution.

In Eq. (7), the oscillation is born from a simple supercritical Hopf bifurcation at oscillation onset. A number of experiments have shown two different values for the oscillation threshold pressure, one for onset and a lower for offset, in a classical hysteresis phenomenon (e.g., Plant et al., 2004; Ruty et al., 2007). In its simplest model, the generation of the hysteresis phenomenon requires a Hopf bifurcation of the subcritical type, in combination with a saddle-node bifurcation between limit cycles (Lucero, 1999), and therefore it cannot be reproduced by the above van der Pol model. However, those two bifurcations and the consequent oscillation hysteresis may be incorporated by simply extending the nonlinear damping term to higher degree polynomials (Ananthkrishnan et al., 1998).

Introducing a similar equation for the left vocal fold (as in Sec. II B), we obtain a system of coupled van der Pol oscillators. Coupling is provided by the term at the right side, which represents the action of the airflow. Again, coupled van der Pol oscillators have been extensively studied (e.g., Kuznetsov et al., 2007, Kuznetsov et al., 2009; Rand and Holmes, 1980; Storti and Rand, 1982), and the theory may be applied to phonation in the presence of vocal asymmetries. In fact, in a recent work (Lucero and Schoentgen, 2013), this modeling strategy was used to obtain regions of phase-locked (1:1 relation) and unlocked oscillation of the coupled system. The results were preliminary in nature and did not consider the full set of oscillatory solutions. Further, the regions were determined in terms of parameters α and $\mu = \beta\lambda$ in Eq. (7). Note that both parameters include subglottal pressure P_s, which complicates the interpretation of the results. Here, the analysis is performed in more detail for the whole set of solutions and expanded with numerical simulations to consider other synchronization regimes.

The linear approximation of P_g is also convenient for voice synthesis. It has been argued that, for sound synthesis applications, a vocal fold model must produce smooth variations of the glottal flow. Non-smoothness increases the content of higher harmonics, which results in unnatural timbres. For example, the popular two-mass model and related lumped representations produce non-smooth variations of the flow at glottal closure and are prone to numerical instabilities when the glottal area is close to zero. Although some techniques have been proposed to solve those issues (Birkholz et al., 2011; Erath et al., 2013; Pelorson et al., 1994), the present model offers a much simpler solution: Division by a small glottal area [when $2x_0 + x_r + x_\ell$ is close to zero, in Eq. (4)] has been eliminated. A smooth glottal closure may be introduced by truncating the glottal area when it is zero (i.e., when $2x_0 + x_r + x_\ell = 0$) with a smooth waveshaper (Lucero et al., 2013; Schoentgen and Lucero,

2013). Synthetic voices produced with this simple model have been assessed by trained clinicians as having a high degree of naturalness.

B. Asymmetric model

We consider first an asymmetry between the normalized stiffness coefficients of the vocal folds, as follows:

$$\ddot{x}_r + \beta(1 + x_r^2)\dot{x}_r + x_r - (\Delta/2)x_r = \alpha(\dot{x}_r + \dot{x}_\ell), \qquad (8)$$

$$\ddot{x}_\ell + \beta(1 + x_\ell^2)\dot{x}_\ell + x_\ell + (\Delta/2)x_\ell = \alpha(\dot{x}_r + \dot{x}_\ell), \qquad (9)$$

where $|\Delta| < 2$ is an asymmetry coefficient. Previous work on asymmetric vocal folds has considered a Q asymmetry quotient which relates the natural frequencies of the left and right vocal folds (e.g., Steinecke and Herzel, 1995). Our modeling simplifies the subsequent analysis because it keeps a constant oscillation frequency independently of the degree of asymmetry. The results may be later expressed in terms of Q by using the relation $Q^2 = (1 + \Delta/2)/(1 - \Delta/2)$. Naturally, several other asymmetric conditions may be introduced by similar *ad hoc* parameters (e.g., see Kuznetsov et al., 2009).

The above model assumes that the glottal pressure resultant from the airflow through the glottis acts on the vocal folds during the whole oscillatory cycle, ignoring any glottal closure. The intention is to analyze first entrainment regimes owing to the aerodynamic coupling. The effect of collision between the vocal folds is considered later in Sec. V B.

III. STABILITY ANALYSIS

A standard stability analysis for the equilibrium position at $x_r = 0$, $x_\ell = 0$ is applied first. The associated characteristic equation is

$$
\begin{aligned}
&s^4 + 2(\beta - \alpha)s^3 + [2 + \beta(\beta - 2\alpha)]s^2 \\
&+ 2(\beta - \alpha)s + 1 - \frac{\Delta^2}{4} = 0,
\end{aligned}
\qquad (10)
$$

where s is a complex variable. This equation has the form $s^4 + a_3 s^3 + a_2 s^2 + a_1 s + a_0 = 0$. When $\alpha = 0$, application of the Routh-Hurwitz criterion shows that all roots have negative real parts and the system is therefore stable. It becomes unstable when one or more roots cross the imaginary axis from left to right. Since $a_0 > 0$ (recall $|\Delta| < 2$), the roots may cross the imaginary axis only in pairs of complex conjugates. Letting $s = \pm i\omega$ and separating real and imaginary parts, we obtain

$$\omega^4 - [2 + \beta(\beta - 2\alpha)]\omega^2 + 1 - \Delta^2/4 = 0, \qquad (11)$$

$$(\beta - \alpha)(\omega^2 - 1) = 0. \qquad (12)$$

Solutions to Eq. (12) are $\beta = \alpha$ and $\omega = 1$. Substituting $\omega = 1$ in Eq. (11) produces

$$\alpha = \frac{\beta}{2} + \frac{\Delta^2}{8\beta}. \qquad (13)$$
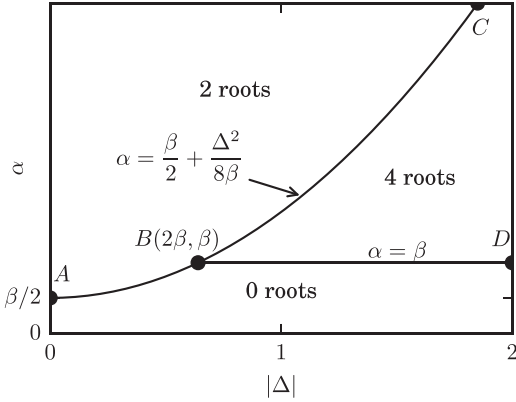
FIG. 1. Results of the stability analysis. The number of complex roots of the characteristic equation with positive real parts is indicated. Curve ABC: Hopf bifurcation. Line BD: Double Hopf bifurcation.

At this condition, a pair of complex conjugate roots cross the imaginary axis.

Next, substituting $\beta = \alpha$ and solving for ω^2,

$$\omega^2 = \left(1 - \frac{\beta^2}{2}\right) \pm \sqrt{\left(1 - \frac{\beta^2}{2}\right)^2 - 1 + \frac{\Delta^2}{4}}, \qquad (14)$$

which has two real solutions for $\beta \geq \sqrt{2}$ and $|\Delta| > 2\beta\sqrt{1 - \beta^2/4}$. Under this condition, two pairs of complex conjugate roots cross the imaginary axis.

Substituting $\beta = \alpha$ in Eq. (13), we obtain the point at which both conditions coincide: $|\Delta| = 2\beta$.

The results are summarized in Fig. 1. In the region below curve AB and line BD, all roots of the characteristic equation have negative real parts. Hence, the equilibrium position is stable, and there are no oscillatory solutions. On curve ABC, a pair of roots of the characteristic equation is purely imaginary and a Hopf bifurcation occurs, which produces a limit cycle. On line BD, the four roots are purely imaginary with values $\pm i\omega_1$ and $\pm i\omega_2$, where $\omega_{1,2}$ are given by the real solutions of Eq. (14), and a double Hopf

bifurcation occurs (Guckenheimer and Holmes, 1983; Guckenheimer and Kuznetsov, 2008). On this line, an invariant two-dimensional torus with periodic or quasi-periodic orbits is produced. The Hopf bifurcation at curve BC is the upper limit of the toroidal region.

IV. PERTURBATION ANALYSIS

A. Averaged equations

We seek now approximations to the oscillatory solutions of Eqs. (8) and (9) by applying an averaging technique (Strogatz, 1994). When $\alpha = 0$ and $\beta = 0$, the system reduces to a pair of uncoupled harmonic oscillators, with the solutions

$$x_r = r_r \cos(t - \theta_r), \quad x_\ell = r_\ell \cos(t - \theta_\ell) \qquad (15)$$

and derivatives

$$\dot{x}_r = -r_r \sin(t - \theta_r), \quad \dot{x}_\ell = -r_\ell \sin(t - \theta_\ell), \qquad (16)$$

where $r_{r,\ell}$ and $\theta_{r,\ell}$ are constants. For small values of α and β, it is reasonable to expect solutions of a similar form, but where $r_{r,\ell}$ and $\theta_{r,\ell}$ are slowly varying functions of time. Therefore, we propose the solution

$$x_r = r_r(t) \cos[t - \theta_r(t)], \qquad (17)$$

$$x_\ell = r_\ell(t) \cos[t - \theta_\ell(t)]. \qquad (18)$$

For the derivatives of Eqs. (17) and (18) to have the same form as in Eq. (16), the condition

$$\dot{r}_r \cos(t - \theta_r) + r_r\dot{\theta}_1 \sin(t - \theta_r) = 0, \qquad (19)$$

$$\dot{r}_\ell \cos(t - \theta_\ell) + r_\ell\dot{\theta}_2 \sin(t - \theta_\ell) = 0, \qquad (20)$$

must hold.

Replacing Eqs. (17) and (18) in Eqs. (8) and (9), and using Eqs. (19) and (20) to solve for $\dot{r}_{r,\ell}$ and $\dot{\theta}_{r,\ell}$, produces expressions of the form

$$2\dot{r}_r = -\sin(t - \theta_r)F[r_r \cos(t - \theta_r), r_r \sin(t - \theta_r), r_\ell \sin(t - \theta_\ell)], \qquad (21)$$

$$2r_r\dot{\theta}_r = \cos(t - \theta_r)F[r_r \cos(t - \theta_r), r_r \sin(t - \theta_r), r_\ell \sin(t - \theta_\ell)], \qquad (22)$$

and similarly for r_ℓ and θ_ℓ. Since r_ℓ and θ_ℓ are slowly varying parameters, they may be approximated by their averages over one cycle of the oscillation, which produces

$$2\dot{r}_r = -\frac{1}{2\pi}\int_0^{2\pi} \sin(t - \theta_r)F[r_r \cos(t - \theta_r), r_r \sin(t - \theta_r), r_\ell \sin(t - \theta_\ell)]\,dt, \qquad (23)$$

$$2r_r\dot{\theta}_r = \frac{1}{2\pi}\int_0^{2\pi} \cos(t - \theta_r)F[r_r \cos(t - \theta_r), r_r \sin(t - \theta_r), r_\ell \sin(t - \theta_\ell)]\,dt. \qquad (24)$$

Computing the integrals and letting $\phi = \theta_r - \theta_\ell$ be the phase difference between the right and left oscillators, we obtain the system of equations

$$2\dot{r}_r = -\beta r_r(1 + r_r^2/4) + \alpha r_r + \alpha r_\ell \cos\phi, \qquad (25)$$

$$2\dot{r}_\ell = -\beta r_\ell(1 + r_\ell^2/4) + \alpha r_\ell + \alpha r_r \cos\phi, \qquad (26)$$

$$2\dot{\phi} = \Delta - \alpha(r_r/r_\ell + r_\ell/r_r)\sin(\phi). \qquad (27)$$

Fixed points of Eqs. (25)–(27) correspond to stationary oscillatory solutions of Eqs. (8) and (9). Setting all derivatives to zero, replacing Eqs. (25) and (26) by their sum and difference, and assuming $r_r + r_\ell \neq 0$ produces

$$-\beta - \frac{\beta}{4}\left(r_r^2 - r_r r_\ell + r_\ell^2\right) + \alpha + \alpha\cos\phi = 0, \qquad (28)$$

$$(r_r - r_\ell)\left[-\beta - \frac{\beta}{4}\left(r_r^2 + r_r r_\ell + r_\ell^2\right) + \alpha - \alpha\cos\phi\right] = 0, \qquad (29)$$

$$\Delta - \alpha(r_r/r_\ell + r_\ell/r_r)\sin\phi = 0. \qquad (30)$$

B. Oscillatory solutions

Equation (29) implies $r_r = r_\ell$ or

$$-\beta - \frac{\beta}{4}\left(r_r^2 + r_r r_\ell + r_\ell^2\right) + \alpha - \alpha\cos\phi = 0. \qquad (31)$$

Letting first $R = r_r = r_\ell$, from Eq. (30) we obtain

$$\sin\phi = \frac{\Delta}{2\alpha}, \qquad (32)$$

which requires $|\Delta| \leq 2\alpha$. For given values of Δ and α, the above equation has two solutions for ϕ: If $\Delta \geq 0$, one solution is in $[0, \pi/2]$ and the other in $[\pi/2, \pi]$; for $\Delta < 0$ the values of ϕ are negative. Further, from Eq. (28),

$$-\beta(1 + R^2/4) + \alpha(1 + \cos\phi) = 0, \qquad (33)$$

which requires

$$\alpha(1 + \cos\phi) \geq \beta. \qquad (34)$$

Let us examine the critical condition $\alpha(1 + \cos\phi) = \beta$. Using Eq. (32) to eliminate ϕ, we arrive at

$$(\beta - \alpha)^2 + \frac{\Delta^2}{4} = \alpha^2, \qquad (35)$$

which produces the same Hopf bifurcation curve given by Eq. (13).

The characteristic equation associated with Eqs. (25)–(27) was computed with the aid of a computer algebra system. For $R = r_r = r_\ell$, the equation is

$$(s - 2\alpha\cos\phi)$$
$$\times \left\{\left[-\beta\left(1 + \frac{3}{4}R^2\right) + \alpha - s\right]^2 - (\alpha\cos\phi)^2\right\} = 0, \qquad (36)$$
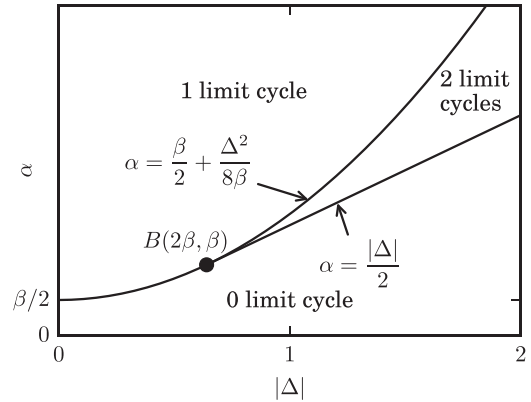

FIG. 2. Regions of existence of oscillatory solutions (limit cycles). When two limit cycles co-exist, one is stable and the other unstable. In case of a unique limit cycle, it is a stable one.

and using Eq. (33) we obtain the roots $s_1 = -2a\cos\phi$, $s_2 = 2\beta - 2\alpha - 2\alpha\cos\phi$, and $s_3 = s_1 + s_2$ (the calculation is straightforward and omitted for brevity). From Eq. (34), $s_2 < 0$. If $\phi \in (-\pi/2, \pi/2)$, then $s_1 < 0$ and so $s_3 < 0$; therefore, the solution is stable. If $\phi \in (-\pi, -\pi/2) \cup (\pi/2, \pi)$, then $s_1 > 0$ and therefore the solution is unstable. Both the stable and unstable solutions become coincident at a saddle-node bifurcation when $\alpha = |\Delta|/2$ and consequently $\phi = \pm\pi/2$. At that bifurcation, the solutions cancel each other.

Equation (13) [equivalent to Eq. (35)] and the condition $\alpha = |\Delta|/2$ define the regions of existence of oscillatory solutions in the $\alpha = |\Delta|$ plane, illustrated in Fig. 2.

Next, assume $r_r \neq r_\ell$ in Eq. (29), so that Eq. (31) holds. Adding and subtracting Eqs. (28) and (31), we obtain

$$r_r^2 + r_\ell^2 = \frac{4(\alpha - \beta)}{\beta} \qquad (37)$$

and

$$\alpha\cos\phi = -\frac{\beta r_r r_\ell}{4}. \qquad (38)$$

From Eq. (30),

$$\alpha\sin\phi = -\frac{\Delta r_r r_\ell}{r_r^2 + r_\ell^2}. \qquad (39)$$

Any solutions produced by the above equations (it may be shown that up to two solutions may exist) are unstable. The characteristic equation has the form (again, the calculation is straightforward and is omitted for brevity)

$$s^3 + As + B = 0, \qquad (40)$$

where A, B are constants. A simple application of the Routh-Hurwitz criterion shows that the equation has one real positive root or two complex roots with positive real parts (note that the coefficient for s^2 is missing), and therefore all solutions are unstable. These solutions will be not analyzed further since they do not have any relevant effect on the dynamics of phase entrainment.

The results of Secs. III–IV B may be combined and summed up in the bifurcation diagram of Fig. 3. Curve ABC
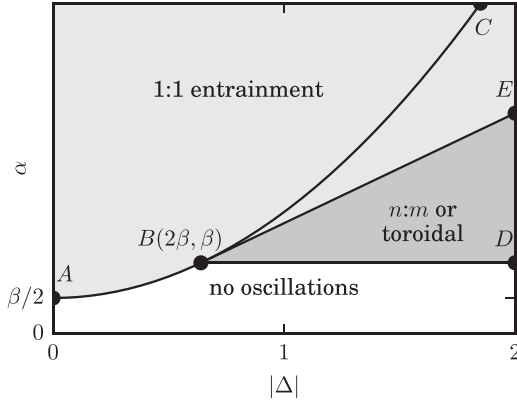
FIG. 3. Bifurcation diagram and regions of oscillation. Curve ABC: Hopf bifurcation, given by Eq. (13). In portion AB the bifurcation is supercritical, and in BC it is subcritical. Curve BE: $\alpha = |\Delta|/2$, saddle-node bifurcation between limit cycles. Line BD: $\alpha = \beta$, double Hopf bifurcation.

is the Hopf bifurcation found in Sec. III. It has both super-critical and subcritical portions, to the left and right of point B, respectively. When the curve is crossed in the upward direction, the equilibrium position becomes unstable and it expels a stable limit cycle, in the supercritical portion, or it absorbs an unstable limit cycle, in the subcritical portion. To the right of point B, there is a region where a stable and an unstable limit cycle co-exist. Note that the stable limit cycle is not produced at the Hopf bifurcation, but at curve BE in a saddle-node bifurcation for limit cycles.

The region of 1:1 phase entrainment is therefore the region of existence of the stable limit cycle. It represents a stable oscillation where both the right and left vocal folds oscillate with the same amplitude R. The amplitude R is given by Eq. (33), and the phase difference ϕ between the vocal folds is given by Eq. (32), with $|\phi| < \pi/2$. Due to our modeling strategy, the oscillation frequency is $\omega = 1$ for any value of Δ. The threshold for this regime (ABE in Fig. 3) increases with $|\Delta|$, meaning that a larger subglottal pressure α is required at larger asymmetries in order to achieve synchronization. Similar shapes for the 1:1 entrainment region are observed in the periodically driven van der Pol oscillator (Mettin et al., 1993) and in other systems of coupled oscillators (Ulrichs et al., 2009).

C. Phase dynamics

It is instructive to explore the dynamics of the oscillation also in terms of a phase equation. Because both oscillators have the same amplitude R, the phase Eq. (27) may be written as

$$\dot{\phi} = \frac{\Delta}{2} - \alpha \sin \phi, \tag{41}$$

which is classical equation of phase dynamics by Adler (1946).

Equilibrium points (fixed points) for the phase are obtained by setting $\dot{\phi} = 0$, which leads to Eq. (32). As previously found, there is a stable fixed point in $(-\pi/2, \pi/2)$ and

an unstable fixed point outside that interval. Both points coincide in a saddle-node bifurcation at $\phi = \pm \pi/2$ when $\alpha = |\Delta|/2$.

When $\Delta = 0$, the phase difference between right and left folds (at the stable solution) is $\phi = 0$. When Δ increases ϕ also increases; i.e., when the right vocal fold becomes more relaxed (less stiff) than the left vocal fold, the oscillation of the right fold becomes delayed in relation to the left one. This result agrees with experiments on physical models of the larynx (Zhang et al., 2013).

It is interesting to note that the range of variation of the phase difference ϕ between the vocal folds follows the so-called "180° rule" of circadian clocks in biology. The rule states that circadian rhythms synchronize to an external timing agent with a phase difference in a 180° range (Granada et al., 2013), independently of the strength of the external agent. In terms of the above phase model, the rule implies that the sensitivity of the phase difference ϕ to the frequency asymmetry Δ depends on the magnitude of the normalized subglottal pressure (or coupling coefficient) α. The higher the subglottal pressure, the smaller the sensitivity; i.e., at a higher subglottal pressure, a mismatch between the natural frequencies of the vocal folds produces a smaller phase difference. At the same time, the range of frequency mismatch over which the vocal folds may synchronize is larger.

The phase model has already been applied to voice production studies for assessing the effect of vocal fold asymmetries on vocal frequency jitter (Schoentgen, 2001).

V. NUMERICAL RESULTS

In Secs. V A–V C, the oscillatory dynamics is further explored through numerical techniques. The equations of the model were first solved in a 200×200 grid spanning the rectangular region $0 \leq \Delta \leq 2$, $0 \leq \alpha \leq 1.5$, and for a time span of 2000 units of normalized time. This time interval was long enough to reach stationarity. The initial transient was removed, and phase entrainment regimes were detected by looking at intersections of trajectories for the right and left oscillators with Poincaré sections in a given direction (Kuznetsov et al., 2007). Here, we used planes at $\dot{x}_r = 0$ and $\dot{x}_\ell = 0$ for each oscillator, in the direction of decreasing $\dot{x}_r$ and $\dot{x}_\ell$, respectively. The entrainment regime was then defined by the relation $n : m$, where n and m are the number of intersections of the right and left trajectories, respectively, with their associated Poincaré sections. Finally, regions of entrainment regimes are presented in the $\Delta \alpha$ plane by coding the $n : m$ relation in gray tones.

A. Effect of stiffness asymmetry

Figure 4(a) shows entrainment regions computed from Eqs. (8) and (9). Predominant regimes are indicated in the graph, and the dark area corresponds to other phase entrainments or toroidal regimes. The numerical results perfectly match the regions found in Fig. 3. Within the $n : m$ regimes (other than 1:1), the most predominant is 3:3, possibly due to presence of a cubic nonlinearity in the differential equations (i.e., $x_r^2 \dot{x}_r$ and $x_\ell^2 \dot{x}_\ell$). In general, the structure of entrainment
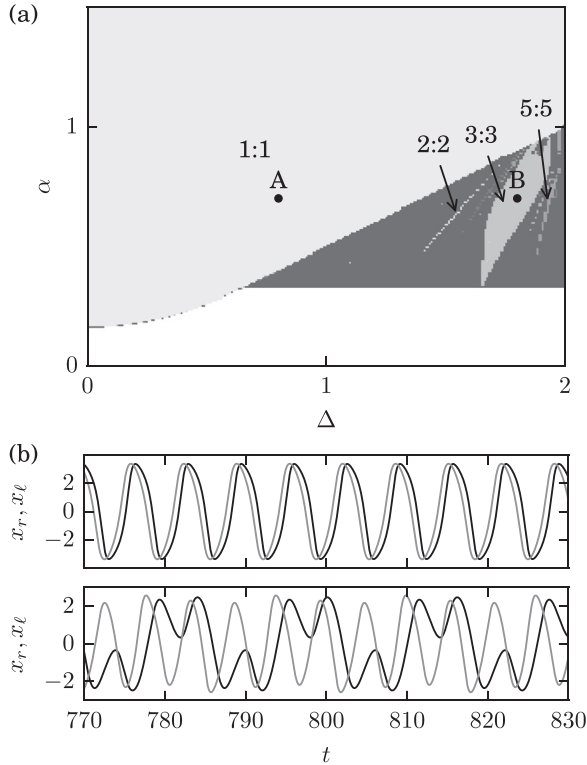
FIG. 4. (a) Entrainment regimes for Eqs. (8) and (9), with $\beta = 0.32$. (b) Solutions corresponding to points A (top) and B (bottom) in plot (a). In (b), the black curves correspond to the right vocal fold and the gray curves correspond to the left one.
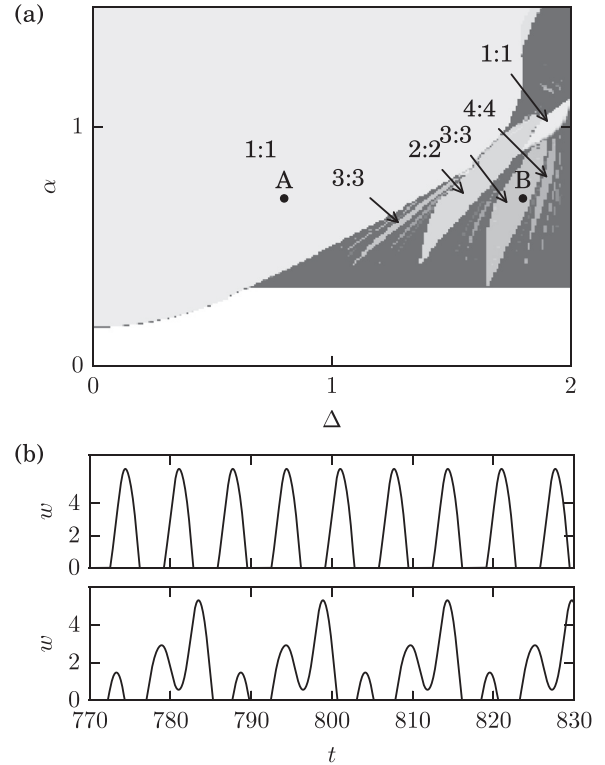
FIG. 5. (a) Entrainment regimes when adding a vocal fold collision model as in Eq. (43), with $x_0 = 1$, $\alpha_c = 0$, and $\beta = 0.32$. (b) Glottal width $w = \max(2x_0 + x_r + x_\ell, 0)$ corresponding to points A (top) and B (bottom) in plot (a).

regimes is similar to the case of the periodically driven van der Pol oscillator (Mettin *et al.*, 1993).

Figure 4(b) shows solutions for the 1:1 region (top) and 3:3 region (bottom). The right vocal fold has a lower stiffness than the left one, and its motion is therefore delayed in time. In the case of the 1:1 entrainment, both folds oscillate with the same amplitude. In the 3:3 regime, both folds have three cycles in one meta-cycle.

B. Effect of collision between the vocal folds

The next figures present results when collision between the opposite vocal folds is added to the model. The collision, and consequent glottal closure, may be simply modeled by letting the glottal pressure in Eq. (2) be

$$P_g = \begin{cases} P_s(a_1 - a_2)/a_1 & \text{if } a_1 > 0 \text{ and } a_2 > 0, \\ P_c & \text{if } a_1 \leq 0 \text{ or } a_2 \leq 0, \end{cases} \quad (42)$$

where P_c is the pressure on the vocal folds during glottal closure. This new definition of the glottal pressure gives the following expression for the right-hand side of Eqs. (8) and (9),

$$\begin{cases} \alpha(\dot{x}_r + \dot{x}_\ell) & \text{if } 2x_0 + x_r + x_\ell > 0, \\ \alpha_c & \text{if } 2x_0 + x_r + x_\ell \leq 0, \end{cases} \quad (43)$$

where x_0 is the normalized value of the glottal half-width and α_c is a normalized pressure for glottal closure. Thus, during the oscillatory cycle, the glottal pressure assumes a different form (a constant value) when the vocal folds come in contact, which introduces an additional coupling between them.

For simplicity, we adopted first $\alpha_c = 0$. An appropriate value of x_0 was then determined as follows. A normal oscillation was simulated with symmetric folds ($\Delta = 0$) and a normalized subglottal pressure α equal to twice the threshold value (soft phonation, Titze, 1992), i.e., $\alpha = 2\beta$. Then, x_0 was selected so as to produce an open quotient of 0.6 (Titze, 1992), which resulted in $x_0 = 1$.

Figure 5(a) shows the resultant entrainment regions. The collision introduces a distortion to the toroidal or $n:m$ region at large asymmetry, and an expanded 2:2 entrainment region. At low and mid asymmetries, on the other hand, no modifications are observed.

Figure 5(b) shows the resultant glottal width for the same parameters as in Fig. 4(b). The top plot corresponds to the 1:1 region, and it shows a train of pulses of constant amplitude with an open quotient of 0.5. The bottom plot corresponds to the 3:3 region; in this case, three glottal pulses occur per glottal meta-cycle.

A larger effect on the vocal fold entrainment is obtained if stronger coupling forces at collision are assumed. Figure 6 shows results when the normalized pressure at glottal closure is increased to $\alpha_c = 20$ while keeping the same value of x_0. The larger value of α_c causes a shorter glottal closure, with an open quotient of 0.9 in the symmetrical case. Nevertheless, larger modifications of the entrainment regions are observed. The 1:1 region has expanded to mid-sized
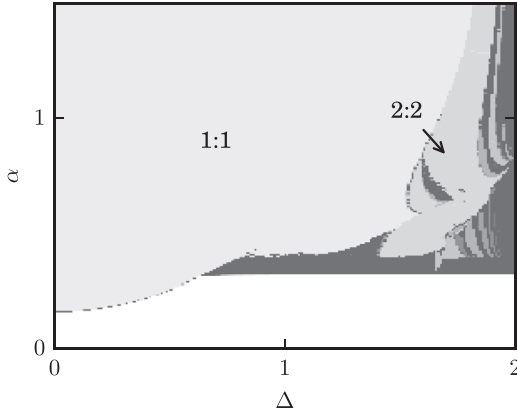
FIG. 6. Entrainment regimes when adding vocal fold collision modeled as in Eq. (43), with $x_0 = 1$, $\alpha_c = 20$, and $\beta = 0.32$.

asymmetries, with the consequence that a lower subglottal pressure α is required to achieve 1:1 entrainment. In addition, the 2:2 region occupies much of the rest of the oscillation region.

C. Effect of damping asymmetry

Finally, we consider the recent finding of a different entrainment region discussed in Sec. I: In a physical model of the vocal folds and at large asymmetry, both folds oscillate in 1:1 entrainment but the lax fold dominates with a large amplitude. The frequency is determined by the lax fold, and the stiff fold follows the lax one with a smaller amplitude (Zhang and Luu, 2012; Zhang et al., 2013).

A similar phenomenon has been detected in coupled van der Pol oscillators, called "broadband synchronization" (Kuznetsov et al., 2007), and consists of one oscillator driving a second passive one. This occurs when the damping coefficients of the oscillators are not identical, e.g.,

$$\ddot{x}_r + \beta_r(1 + x_r^2)\dot{x}_r + x_r - (\Delta/2)x_r = \alpha(\dot{x}_r + \dot{x}_\ell), \quad (44)$$

$$\ddot{x}_\ell + \beta_\ell(1 + x_\ell^2)\dot{x}_\ell + x_\ell + (\Delta/2)x_\ell = \alpha(\dot{x}_r + \dot{x}_\ell), \quad (45)$$

with $\beta_r < \beta_\ell$. Thus, the subglottal pressure (α) may be strong enough to cause self-excited oscillations of the right oscillator, which drives but is not able to overcome the damping of the left oscillator, which behaves as a passive damped system.

As an example, this phenomenon was simulated by letting $\beta_\ell = 2\beta_r$ and all other parameters as in Sec. V A with the results shown in Fig. 7. A substantial modification in the entrainment regions is observed: The region of 1:1 entrainment has expanded to low values of α covering the full range of Δ.

Figure 7(b) shows the solution in the 1:1 region at the lower right of the diagram in Fig. 7(a). Note that the left vocal fold has much smaller amplitude than the right one. Comparing to the plots in Fig. 4(b) we also see that the oscillation frequency is lower. The period is $T = 15.13$, which implies an angular frequency of $\omega = 2\pi/T = 0.41$. This value is close to the natural frequency of the right (softer)
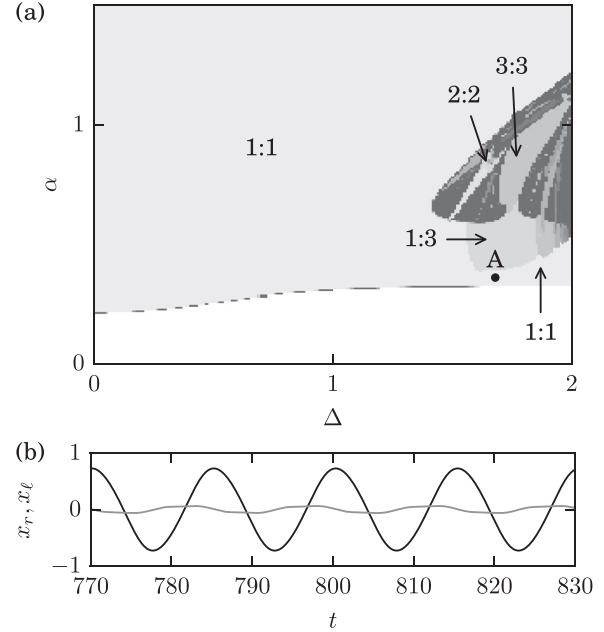

FIG. 7. (a) Entrainment regimes for Eqs. (44) and (45), with $\beta_r = 0.32$, $\beta_l = 0.64$. (b) Solutions corresponding to point A in plot (a). In (b), the black curve corresponds to the right vocal fold and the gray curve corresponds to the left one.

oscillator $\omega = \sqrt{1 - \Delta/2} = 0.40$. These characteristics match perfectly the findings by Zhang and Luu (2012). On the other hand, the phase difference is large (about 90°), but it is not the anti-phase found in their experiments.

Let us note that in their work, Zhang and Luu (2012) adopted a continuum model of the vocal folds to simulate the observed regimes. An oscillation with a dominant lax fold was obtained by setting a large stiffness asymmetry between the right and left folds. However, the model assumed a tissue damping proportional to the mass and to the natural frequency. In that case, a stiffness asymmetry implies a damping asymmetry (for equal masses of the right and left folds) in which the lax fold has a lower damping. Therefore, our modeling above agrees with approach of Zhang and Luu (2012).

On the other hand, the continuum model has also been used to characterize the onset of the vocal fold oscillation in terms of the synchronization of different oscillation eigenmodes (Zhang et al., 2007). Thus, a stiffness asymmetry could result in different oscillation threshold values of the subglottal pressure for the right and left vocal folds, when considered separately. It might be possible, therefore, to reproduce the above phenomenon by means of a stiffness asymmetry alone.

VI. EXPERIMENTAL VALIDATION

Experimental support may be given to the above theoretical results by using measurements from a mechanical replica of the vocal folds. The replica has been described in detail elsewhere (Ruty et al., 2007; Pelorson and Laval, 2012; Pelorson et al., 2013).

Briefly, it consists of two parallel latex sleeves filled with water under pressure and supported by a metallic structure.
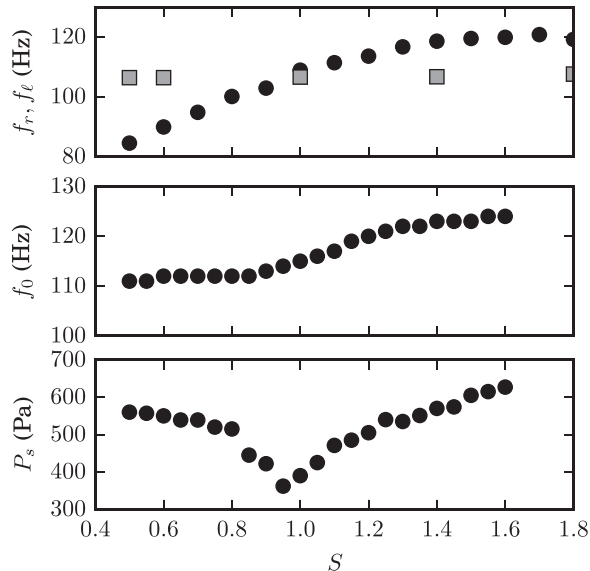
J. Acoust. Soc. Am., Vol. 137, No. 4, April 2015

Lucero et al.: Self-entrainment of the vocal folds   2043

FIG. 8. Measured data as a function of the ratio S of water pressure inside the latex sleeves representing the vocal folds. Top: First natural frequencies of the sleeves. The squares represent the sleeve with a constant water pressure, and the circles represent the sleeve with a varying pressure. Middle: Oscillation frequency at onset. Bottom: Upstream pressure at oscillation onset.

The latex sleeves represent the vocal folds in a 3:1 scale. Air from a pressure reservoir is blown through a third latex sleeve, representing the glottal passage, situated in-between the two vocal fold sleeves and perpendicular to them. Given enough air pressure, an oscillation of the sleeves may be excited, reproducing the behavior of the human vocal folds during phonation. A pressure sensor (XCS-093, Kulite Semiconductor Products Inc., Leonia, NJ) measures the air pressure immediately upstream the sleeves. Calibration of the pressure sensor was made against a water meter with an accuracy of ± 5 Pa.

Measures of oscillation threshold pressure were obtained by increasing the air pressure upstream of the replica from zero until an oscillation of the sleeves was detected. The time instant of oscillation onset was determined by spectral analysis of the upstream pressure signal, and the mean upstream pressure and oscillation frequency at that instant were computed (for details on the measurement process, see Lucero et al., 2012b). The process was repeated for various values of internal water pressure of one of the vocal fold sleeves, while keeping constant the water pressure in the other sleeve.

The final data set consisted of 23 triplets $(S, f_{\text{on}}, P_{\text{on}})$ where S is the ratio of water pressures inside the sleeves, f_{on} is the fundamental frequency of the oscillation at onset, and P_{on} is the upstream oscillation threshold pressure. In addition, the mechanical response of the replica was measured by means of a shaker whose probe is equipped with an accelerometer in conjunction with a laser vibrometer. Thus, the natural frequencies of the vocal fold sleeves were determined for various water pressure configurations. The first (lowest) natural frequency was closer to the oscillation frequency than the others, and was therefore selected for the analysis below. Repeated measurements showed less than 1% of variability for the first natural frequency, indicating a
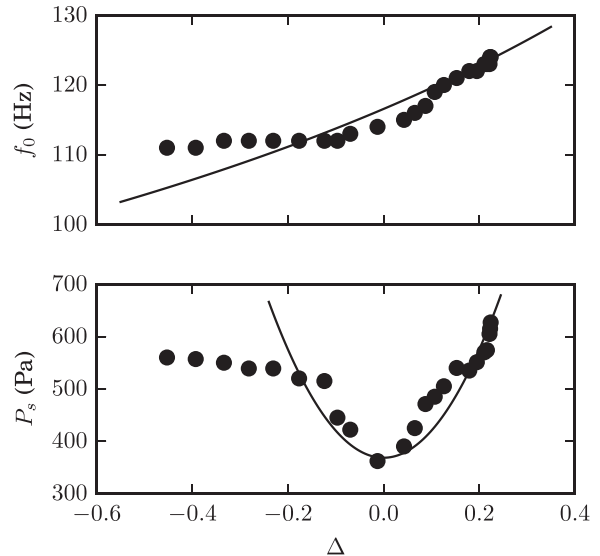

FIG. 9. Oscillation frequency (top) and upstream pressure (bottom) vs coefficient of asymmetry. Circles: Measured data, curves: Theoretical model.

good level of measurement repeatability. Figure 8 shows the measured data.

In Eqs. (8) and (9), the natural angular frequencies of the oscillators are given by $\omega_{r,\ell}^2 = 1 \mp \Delta/2$. Therefore, the ratio of natural frequencies is $Q = \sqrt{(1 + \Delta/2)/(1 - \Delta/2)}$. Solving for Δ we obtain

$$\Delta = 2\left(\frac{Q^2 - 1}{Q^2 + 1}\right). \tag{46}$$

In the case of 1:1 entrainment, the oscillation angular frequency of the coupled system is given by $\omega_0^2 = (\omega_r^2 + \omega_\ell^2)/2 = (\omega_r^2/2)(1 + Q^2)$. Assuming that the stiffness of the right oscillator is kept constant, the oscillation frequency may be expressed as

$$f_0 = a\sqrt{1 + Q^2}, \tag{47}$$

where $a = \omega_r^2/2$.

We may use Eq. (13) to compute the threshold pressure for small asymmetries. Replacing α and β and solving for the subglottal pressure, we obtain

$$P_s = b + c\Delta^2, \tag{48}$$

where $b = Bx_0/(2\tau)$ and $c = x_0 MK/(8B\tau)$.

Equations (47) and (48) were fitted to the measured data as follows. The relation $Q = f(S)$ was computed from the top plot in Fig. 8 by interpolation. Coefficient b in Eq. (48) was next estimated by interpolation from the middle plot as the value of P_s for $Q = 1$, with the result $b = 371.3$ Pa. Finally, optimal values of coefficients $a = 82.5$ Hz and $c = 4\,800.7$ Pa were determined by applying a standard least squares procedure. The results of the fit are shown in Fig. 9. In the case of coefficient c for the onset pressure (bottom plot), the optimal value was computed by neglecting the five leftmost data points. Note that the measured data do not show a symmetric pattern for negative and positive values of

Lucero et al.: Self-entrainment of the vocal folds

Δ: For negative values, both the oscillation frequency and the oscillation onset tend to constant values (to the left of the plots). Therefore, the model fails to provide a good fit in that region. Outside that region, the model provides a good fit; the R^2 coefficients are 0.79 and 0.77 for the frequency and the pressure, respectively.

VII. CONCLUSIONS

This article presents a simple theoretical model to characterize entrained oscillations of the right and left vocal folds in the presence of asymmetries. The simplicity of the model enables an analytical treatment of the oscillations, and also a link to other classical models of coupled oscillations in physiology, such as the van der Pol oscillator and Adler's equation of phase dynamics.

The analysis has shown that a stiffness asymmetry between the left and right vocal folds increases the subglottal threshold pressure in the 1:1 entrainment region. Within this region, both vocal folds oscillate with the same amplitude at a common oscillation frequency equal to the average of the natural frequencies of the folds, and with the lax fold delayed in time with regard to the tense fold. At large asymmetries, a region of toroidal or higher $n:m$ entrainment regimes appears, with a constant threshold pressure.

The mathematical analysis has only considered the coupling provided by the airflow through the glottis. When collisions between opposite folds during the oscillatory cycle are introduced, the 1:1 entrainment region is expanded toward a lower subglottal threshold pressure. Also, the region of toroidal or $n:m$ entrainment regimes is distorted and replaced by a 2:2 regime.

When an asymmetry in the damping coefficients of the oscillators is introduced (so that the oscillator with the lowest damping also has the lowest natural frequency), then a broadband synchronization phenomenon is observed. This phenomenon expands the 1:1 regime to low subglottal pressures across the whole stiffness asymmetry range. In the expanded region, the oscillator with the lowest natural frequency is dominant: It has large amplitude and the oscillation frequency is close to its natural frequency. The other oscillator follows the oscillation with a large phase advance and a very small amplitude.

The theoretical findings match observations of asymmetrical vocal fold oscillations and data from measurements on mechanical replicas. Particularly, we have shown that the model fits data from a latex replica of the vocal folds with good accuracy, at low asymmetries.

Limitations of the results due to simplifications of the vocal fold model must also be considered. For example, the model assumes oscillations with a single degree of freedom for each fold. Actual motion of the vocal folds includes components in three-dimensional directions and may combine various oscillation eigenmodes (Zhang *et al.*, 2007). The model is also quasi-linear and assumes a linear elastic restoring force for the tissues as well as a linear approximation of the glottal pressure. Therefore, it may not be valid for cases of very large oscillation amplitudes and high subglottal pressures. Finally, the effect of the vocal tract has been neglected. It has been reported that resonant effects of the vocal tract may enhance vocal instabilities and reduce regions of phase entrainment (Mergell and Herzel, 1997).

Adler, R. (**1946**). "A study of locking phenomena in oscillators," Proc. IRE **34**, 351–357.

Ananthkrishnan, N., Sudhakar, K., Sudershan, S., and Agarwal, A. (**1998**). "Application of secondary bifurcations to large amplitude limit cycles in mechanical systems," J. Sound Vib. **215**, 183–188.

Arneodo, E. M., and Mindlin, G. B. (**2009**). "Source-tract coupling in birdsong production," Phys. Rev. E **79**, 061921.

Berry, D. A., Herzel, H., Titze, I. R., and Story, B. H. (**1996**). "Bifurcations in excised larynx experiments," J. Voice **10**, 129–138.

Birkholz, P., Kröger, B. J., and Neuscheafer-Rube, C. (**2011**). "Synthesis of breathy, normal, and pressed phonation using a two-mass model with a triangular glottis," in *Interspeech 2011*, Florence, Italy, pp. 2681–2684.

Cartwright, M. L. (**1960**). "Balthazar van der Pol," J. London Math. Soc. **s1-35**, 367–376.

Edelstein-Keshet, L. (**2005**). *Mathematical Models in Biology* (SIAM, Philadelphia, PA), Chap. 8, pp. 333–341.

Erath, B. D., Sommer, D. E., Zañartu, M., and Peterson, S. D. (**2013**). "Nonlinearities in block-type reduced-order vocal fold models with asymmetric tissue properties," Proc. Mtg. Acoust. **19**, 060243.

Eysholdt, U., Rosanowski, F., and Hoppe, U. (**2003**). "Vocal fold vibration irregularities caused by different types of laryngeal asymmetry," Eur. Arch. Otorhinolaryngol. **260**, 412–417.

Glass, L. (**2001**). "Synchronization and rhythmic processes in physiology," Nature **410**, 277–284.

Glass, L., and Mackey, M. C. (**1988**). *From Clocks to Chaos* (Princeton University Press, Princeton, NJ), Chap. 7, pp. 119–143.

Granada, A. E., Bordyugov, G., Kramer, A., and Herzel, H. (**2013**). "Human chronotypes from a theoretical perspective," PloS One **8**, e59464.

Grimshaw, R. (**1991**). *Nonlinear Ordinary Differential Equations* (CRC Press, Boca Raton, FL), Chap. 6, pp. 153–164.

Guckenheimer, J., and Holmes, P. (**1983**). *Nonlinear Oscillations, Dynamical Systems, and Bifurcations of Vector Fields* (Springer, New York), Chap. 7, pp. 364–376.

Guckenheimer, J., and Kuznetsov, Y. A. (**2008**). "Hopf-Hopf bifurcation," Scholarpedia **3**, 1856. Online at http://scholarpedia.org/article/Hopf-Hopf_bifurcation (Last viewed September 7, 2014).

Herzel, H., and Knudsen, C. (**1995**). "Bifurcations in a vocal fold model," Nonlinear Dyn. **7**, 53–64.

Ishizaka, K., and Isshiki, N. (**1976**). "Computer simulation of pathological vocal-cord vibration," J. Acoust. Soc. Am. **60**, 1193–1198.

Kuznetsov, A. P., Paksyutov, V. I., and Roman, R. Y. (**2007**). "Features of the synchronization of coupled van der Pol oscillators with nonidentical control parameters," Tech. Phys. Lett. **33**, 636–638.

Kuznetsov, A. P., Stankevich, N. V., and Turukina, L. V. (**2009**). "Coupled van der Pol-Duffing oscillators: Phase dynamics and structure of synchronization tongues," Physica D **238**, 1203–1215.

Laje, R., Gardner, T., and Mindlin, G. B. (**2001**). "Continuous model for vocal fold oscillations to study the effect of feedback," Phys. Rev. E **64**, 056201.

Laje, R., Gardner, T. J., and Mindlin, G. B. (**2002**). "Neuromuscular control of vocalizations in birdsong: A model," Phys. Rev. E **65**, 051921.

Lucero, J. C. (**1999**). "Theoretical study of the hysteresis phenomenon at vocal fold oscillation onset-offset," J. Acoust. Soc. Am. **105**, 423–431.

Lucero, J. C., Koenig, L. L., and Fuchs, S. (**2012a**). "Modeling source-tract interaction in speech production: Voicing onset vs. vowel height after a voiceless obstruent," in *Interspeech2012*, Portland, OR, pp. 2198–2201.

Lucero, J. C., Koenig, L. L., Lourenço, K. G., Ruty, N., and Pelorson, X. (**2011**). "A lumped mucosal wave model of the vocal folds revisited: Recent extensions and oscillation hysteresis," J. Acoust. Soc. Am. **129**, 1568–1579.

Lucero, J. C., Lourenço, K. G., Hermant, N., Hirtum, A. V., and Pelorson, X. (**2012b**). "Effect of source-tract acoustical coupling on the oscillation onset of the vocal folds," J. Acoust. Soc. Am. **132**, 403–411.

Lucero, J. C., and Schoentgen, J. (**2013**). "Modeling vocal fold asymmetries with coupled van der Pol oscillators," Proc. Mtg. Acoust. **19**, 060165.

Lucero, J. C., Schoentgen, J., and Behlau, M. (**2013**). "Physics-based synthesis of disordered voices," in *Interspeech2013*, Lyon, France, pp. 587–591.

Mergell, P., and Herzel, H. (**1997**). "Modelling biphonation—The role of the vocal tract," Speech Commun. **22**, 141–154.

Mergell, P., Herzel, H., and Titze, I. R. (**2000**). "Irregular vocal-fold vibration—High-speed observation and modeling," J. Acoust. Soc. Am. **108**, 2996–3002.

Mettin, R., Parlitz, U., and Lauterborn, W. (**1993**). "Bifurcation structure of the driven van der Pol oscillator," Int. J. Bifurcat. Chaos **3**, 1529–1555.

Pelorson, X., Hirschberg, A., Vanhassel, R. R., Wijnands, A. P. J., and Auregan, Y. (**1994**). "Theoretical and experimental study of quasi-steady-flow separation within the glottis during phonation. Application to a modified 2-mass model," J. Acoust. Soc. Am. **96**, 3416–3431.

Pelorson, X., Hirtum, A. V., Wu, B., and Silva, F. (**2013**). "Theoretical and experimental study of glottal geometry in phonation," Proc. Mtg. Acoust. **19**, 035044.

Pelorson, X., and Laval, X. (**2012**). "An experimental replica of the vocal folds to study normal and pathological voice," in *Proceedings of the Acoustics*, Nantes, France, pp. 1755–1759.

Pikovsky, A., Rosenblum, M., and Kurths, J. (**2001**). *Synchronization—A Universal Concept in Nonlinear Sciences* (Cambridge University Press, Cambridge), Chap. 1, p. 23.

Plant, R. L., Freed, G. L., and Plant, R. E. (**2004**). "Direct measurement of onset and offset phonation threshold pressure in normal subjects," J. Acoust. Soc. Am. **116**, 3640–3646.

Rand, R. H., and Holmes, P. J. (**1980**). "Bifurcations of periodic motions in two weakly coupled van der Pol oscillators," Int. J. Nonlinear Mech. **15**, 387–399.

Ruty, N., Pelorson, X., Van Hirtum, A., Lopez-Arteaga, I., and Hirschberg, A. (**2007**). "An *in vitro* setup to test the relevance and the accuracy of low-order vocal folds models," J. Acoust. Soc. Am. **121**, 479–490.

Schoentgen, J. (**2001**). "Stochastic models of jitter," J. Acoust. Soc. Am. **109**, 1631–1650.

Schoentgen, J., and Lucero, J. C. (**2013**). "Synthesis by rule of disordered voices," in *Advances in Nonlinear Speech Processing*, edited by T. Drugman and T. Dutoit (Springer-Verlag, Berlin), pp. 120–127.

Schwarz, R., Hoppe, U., Schuster, M., Wurzbacher, T., Eysholdt, U., and Lohscheller, J. (**2006**). "Classification of unilateral vocal fold paralysis by endoscopic digital high-speed recordings and inversion of a biomechanical model," IEEE Trans. Biomed. Eng. **53**, 1099–1108.

Smith, M. E., Berke, G. S., Gerratt, B. R., and Kreiman, J. (**1992**). "Laryngeal paralyses: Theoretical considerations and effects on laryngeal vibration," J. Speech Hear. Res. **35**, 545–554.

Steinecke, I., and Herzel, H. (**1995**). "Bifurcations in an asymmetric vocal-fold model," J. Acoust. Soc. Am. **97**, 1874–1884.

Storti, D. W., and Rand, R. H. (**1982**). "Dynamics of two strongly coupled van der Pol oscillators," J. Nonlinear Mech. **17**, 143–152.

Strogatz, S. H. (**1994**). *Nonlinear Dynamics and Chaos* (Westview Press, Boulder, CO), Chap. 7, pp. 215–227.

Tigges, M., Mergell, P., Herzel, H., Wittenberg, T., and Eysholdt, U. (**1997**). "Observation and modelling of glottal biphonation," Acta Acust. Acust. **83**, 707–714.

Titze, I. R. (**1988**). "The physics of small-amplitude oscillation of the vocal folds," J. Acoust. Soc. Am. **83**, 1536–1552.

Titze, I. R. (**1992**). "Phonation threshold pressure: A missing link in glottal aerodynamics," J. Acoust. Soc. Am. **91**, 2926–2935.

Titze, I. R. (**1994**). *Principles of Voice Production* (Prentice-Hall, Englewood Cliffs, NJ), pp. 285–286.

Ulrichs, H., Mann, A., and Parlitz, U. (**2009**). "Synchronization and chaotic dynamics of coupled mechanical metronomes," Chaos **19**, 043120.

Wilden, I., Herzel, H., Peters, G., and Tembrock, G. (**1998**). "Subharmonics, biphonation, and deterministic chaos in mammal vocalization," Bioacoustics **9**, 171–196.

Zhang, Y., and Jiang, J. J. (**2004**). "Chaotic vibrations of a vocal fold model with a unilateral polyp," J. Acoust. Soc. Am. **115**, 1266–1269.

Zhang, Z. (**2010**). "Vibration in a self-oscillating vocal fold model with left-right asymmetry in body-layer stiffness," J. Acoust. Soc. Am. **128**, EL279–EL285.

Zhang, Z., Kreiman, J., and Gerratt, B. R. (**2013**). "Acoustic and perceptual effects of changes in body layer stiffness in symmetric and asymmetric vocal fold models," J. Acoust. Soc. Am. **133**, 453–462.

Zhang, Z., and Luu, T. H. (**2012**). "Asymmetric vibration in a two-layer vocal fold model with left-right stiffness asymmetry: Experiment and simulation," J. Acoust. Soc. Am. **132**, 1626–1635.

Zhang, Z., Neubauer, J., and Berry, D. A. (**2007**). "Physical mechanisms of phonation onset: A linear stability analysis of an aeroelastic continuum model of phonation," J. Acoust. Soc. Am. **122**, 2279–2295.